Quaternary International 660 (2023) 21–30

Contents lists available at ScienceDirect

Quaternary International

journal homepage: www.elsevier.com/locate/quaint

Investigating diagenesis of archaeological bones from Etton Causewayed enclosure, UK

Charlotte Loy, Fiona Brock *, Chris Dyer

Cranfield Forensic Institute, Cranfield University, Defence Academy of the United Kingdom, Shrivenham, SN6 8HR, UK

ARTICLE INFO

Keywords:
Bone diagenesis
Manganese
Iron
Taphonomy
Redox conditions

ABSTRACT

Diagenesis of archaeological bones proceeds via a complex combination of chemical, physical and/or microbial processes often over several millennia. These processes are influenced by the depositional environment, including fluctuations in pH, mineral availability and water table. This study investigates diagenetic alterations to the mineral and organic (collagen) phases of bones from a Neolithic site, Etton Causewayed Enclosure (Cambridgeshire, UK). Archaeological bones from some layers of the gravel site at Etton exhibit unusual staining patterns, including iron and manganese rich layers underneath the exterior bone surface and manganese speckling throughout the bone. A range of analytical techniques (micro-CT, FTIR, XRF and SEM-EDS) were employed to investigate the mineralisation within three bones from this site. Diagenesis appears to have occurred through a combination of bacterial degradation and mineral formation due to the changing redox conditions at the site caused by fluctuating groundwater. The reason for the positioning of the manganese layers beneath the iron layers at the surfaces of the bone remains unclear.

1. Introduction

The breakdown of bones after death and deposition is a wide ranging and varied process, depending upon the burial environment and a multitude of associated factors. The taphonomic degradation of bone follows general rules based on the depositional environment. The pH, hydrology and soil composition of a site have great bearing on what chemical reactions and organisms are present to modify the bone (e.g. Nielsen-Marsh et al., 2007; Fernández-Jalvo et al., 2010). Sites with permeable soils like sands and gravels are frequently recharged with fresh water, which is undersaturated with calcium and phosphate, resulting in increased bone demineralisation (e.g. Hedges, 2002; Nielsen-Marsh and Hedges, 2000), as well as an influx of ions such as manganese, iron and nitrates.

Diagenesis of bone covers multiple processes from possible scavenging and burial, to perhaps eventual fossilisation. The following is a description of some of the general overlapping factors in this process. In general terms soft tissue first decomposes or is picked off the bone by scavengers. The bone can be buried immediately or over a period of time become buried. Post mortem breaks are common. Microscopic attack ensues with bacteria, fungi, moss, root action, algae, lichen and more all being known to alter bone structure (Fernández-Jalvo et al., 2010). The organic component of bone tissue, mainly collagen, degrades over time and the inorganic crystalline component increases, often in spaces now available in the bone tissue (Kiseleva et al., 2019; Child, 1995; Herwartz et al., 2013; Dal Sasso et al., 2014). Exogenous substances can migrate into bone tissue, especially if spaces start to form from the loss of protein content (e.g. Badone and Farquhar, 1982; White and Booth, 2014; Trueman et al., 2008).

Iron and manganese are commonly present in groundwater and are often involved in bone diagenesis, notably in fossilisation (Henne et al., 2021; Elliot and Grime, 1993; Badone and Farquhar, 1982; Kiseleva et al., 2019). Manganese and iron often exist on, and within, bones as a collection of oxides and hydroxides (Marín Arroyo et al., 2008). In archaeology, manganese staining is often seen within bone and stone deposits in caves, and most often on the outside surface of the material (Marín Arroyo et al., 2008). However, it is often assumed the visual deposits are superficial and rarely the extent of the manganese material into the bone is confirmed. Iron and manganese can be incorporated passively onto and into bone and stone, often visualised as direct diffusion into the entire bone; they may also be introduced via fluctuations in reducing and oxidising (redox) environments, mobilising soluble metal ions and then reforming them elsewhere (Elliot and Grime, 1993; Breuning-Madsen et al., 2001). Bacterial action has been noted as

* Corresponding author.
E-mail address: f.brock@cranfield.ac.uk (F. Brock).

https://doi.org/10.1016/j.quaint.2022.12.012
Received 3 May 2022; Received in revised form 21 December 2022; Accepted 26 December 2022
Available online 2 January 2023

a likely cause of available manganese and possible facilitator of its formation in bone, however there is no conclusive evidence for this type of formation in archaeological bone (Marín Arroyo et al., 2008; Dal Sasso et al., 2014).

The term 'Microscopical Focal Destruction' (MFD) has been used to describe regions of bone relating to areas of destruction, often surrounded by a hypermineralised 'cuff' of processed bone material (Hackett, 1981; White and Booth, 2014). These are normally associated with bacteria, which have been described as 'reorganizing' the bone mineral as well as destroying it (Jans, 2010; Turner-Walker, 2019). While the complex differentiated types of microbial destruction have been called into question, the typical periosteal and endosteal degradation seen in archaeological bone is widely believed to be bacterially-mediated (Turner-Walker, 2019; Fernández-Jalvo et al., 2010; Booth et al., 2016).

In this study four complementary analytical techniques (X-ray fluorescence, scanning electron microscopy, FTIR spectroscopy and micro-CT scanning) were utilised to assess the diagenetic alterations to archaeological bones found in a peat-rich gravel site with a fluctuating water table. The bones from the Neolithic site of Etton Causewayed Enclosure, are – to the authors' knowledge - unique, exhibiting peculiar internal staining of rich mineralised orange/red and black-coloured layers beneath an apparently unchanged exterior buff-coloured surface, followed by dark speckling deeper into the bone. On the endosteal (inner) edge these mineral layers are repeated. The hard tissue itself visually looks smooth and undisturbed. Although some rare archaeological examples do show surface iron layering and manganese speckling in cross section of bone (Reiche et al., 2003), we are not aware of any direct parallel from other archaeological sites to the multiple layers and mineralisation patterns observed in the bones from Etton.

2. Materials and methods

2.1. The archaeological site and excavated bone

Near the villages of Maxey and Etton in Cambridgeshire, East Anglia, UK (OS NGR TF 13830739; GPS co-ordinates: 52.652675, −0.323974), was a sand and gravel Neolithic Causewayed Enclosure that once existed on a low-lying island in a fen from the first half of the 4th millennium BC (5950- 5450 BP). The site had an extensive history of repeated seasonal flooding and was eventually abandoned, likely as the water levels became too high (Pryor, 1998). Excavations took place between 1982 and 1987, revealing ca. 80% of the interior of the enclosure. Bones found appear to be butchery remains (in particular cattle) from the seasonal living and ritual deposition at the site. On excavation, the bones were washed in tap water; limited cleaning was required as the sandy loam soils adhering to the surface fell away easily, while the secondary iron surface deposits were not easily removed (C. French, *pers. comm.* 2022). Following air drying, the bones were placed in fresh paper bags and boxed for long-term storage.

A minority of bones from a ditch dated to the later Neolithic period showed the unusual mineralisation patterns described above. Of the seven bones that clearly exhibited these mineralisation patterns, three representative specimens (E781, E11525 and E12313; Fig. 1) were chosen for intensive study. Sample E11525 is identified as bovine, but E781 and E12313 have not been identified to species. The remaining bones from the ditch showed diagenesis typical of anoxic environments, many being stained brown (Kendall et al., 2018; Pryor, 1998). Root etching marks are still visible on some of the bone surfaces, showing this outer layer was the one in contact with the ground when buried.

Fig. 1. Three bones showing unusual mineralisation patterns, including orange/brown and black layers interior to the periosteal and endosteal edges, and black mottling of the interior bone. Images a, b, c: sample E781; d, e, f; sample E11525; g, h, i: sample E12313. (For interpretation of the references to colour in this figure legend, the reader is referred to the Web version of this article.)

2.2. Sample preparation

The analysis undertaken in this study was performed as a precursor for synchrotron analysis (not reported here). With this in mind, thin sections (230–330 μm) of each bone were taken with a Buehler IsoMet™ low speed, water cooled, diamond blade microtome, at setting 4 or 4.5. The XRF, SEM-EDS and FTIR analysis described below was undertaken on these fragile thin cross sections of bone, which were studied unpolished to preserve their integrity and avoid pulling out mineral fragments. For the micro-CT the remaining whole bone was scanned.

2.3. X-ray fluorescence spectrometry (XRF)

The elemental compositions of the stained regions were assessed using a benchtop SciMed SEA6000VX X-ray fluorescence spectrometer. Measurements were taken over a 0.2 × 0.2 mm area in air at the instrument's normal focusing distances, with its X-ray tube operating at 50 kV and 1000 μA, without any filtration. Measurements were taken with a pixel size of 30 μm and time spent per pixel as 50 ms, to generate elemental maps (Ca, P, Mn, Fe) of the thin sections of bone. Scan sizes were as follows: 8.64 × 12.81 mm (E781), 6.7 × 13.02 mm (E11525) and 9.63 × 13.02 mm (E12313).

2.4. Scanning electron microscopy (SEM-EDS)

A Hitachi SU3500 scanning electron microscope with an attached EDAX microanalysis system (running TEAM software) was used to investigate the composition of the bone material and mineral infills. The unpolished thin sections of bone were prepared for synchrotron analysis, and so could not be surface coated for high vacuum SEM as the coating would interfere with subsequent analysis, which reduced the resolution, making it difficult to visualise changes in bone histology and evidence of bioerosion. The machine operating conditions were a voltage of 15 kV, a spot intensity of 70, a vacuum pressure of 80 Pa, all in Variable Pressure (VP) mode.

2.5. Micro-computed tomography (Micro-CT)

Micro-CT scanning was undertaken using a Nikon Metris XT H 225 scanner with a tungsten reflectance target. The working conditions for each scan were an accelerating voltage of 100 kV, a current of 45–50 μA and an exposure time of 500 ms. The instrument was set to optimise projections (typically 1471), with 2 frames per projection. The resultant voxel size ranged between 69.3 and 121.4 μm for the largest fragments, and 15.1–33.9 μm for the smaller fragments. The software used to reconstruct the data was CT Pro 3D (Nikon Metrology, UK) and data was visualised and processed using VG StudioMax 2.1. (Volume Graphics, GmbH, Germany).

2.6. Fourier transform infra-red (FTIR) spectroscopy

FTIR analysis was carried out using a Spotlight 200 attached to a Spectrum 100 benchtop instrument (both PerkinElmer) with a mid-IR optimised source, beamsplitter and a liquid nitrogen-cooled MCT detector in microscope mode. Spectra were collected in the mid-infrared wavelength at 800-4000 cm^{-1}.

The microscope feature of the FTIR allowed spectra to be collected from targeted areas within three differently-coloured regions of thin sections of each bone: red/orange (i.e. iron-rich), dark (i.e. manganese-rich), or unstained regions. A minimum of 6 spectra were collected from each of these three different regions per sample, with an average of 7.4 scans taken per region per bone, and a total of 67 spectra collected. The aperture size (i.e. the area scanned for each spectrum) was kept at 50 × 50 μm where possible to allow small features to be studied, but was increased to 100 × 100 μm for nine spectra. The number of scans collected for each spectrum depended on the sample itself, and was chosen to optimise peak signals and reduce interference. For most samples, 115 scans were collected, but some regions required as few as 10 scans to generate clear spectra, while the sections from E781 required 250 scans. A gold mirror was used as the background material in the reflectance spectra. A new background was run after every change in scan number, aperture size, or thin section.

The software used to view and transform the data were PerkinElmer Spectrum 10.5.4, PerkinElmer Spectrum image and Spectragryph version v1.2.6. Due to the thickness of the samples, total reflectance was measured, with no separation between the diffuse and specular components. A Kramers-Kronig transformation was used to convert the reflectance data into absorbance data.

The presence of organic material and bone mineral carbonate in the 'red/orange' iron- and 'dark' manganese-rich regions of bone, as well as the 'off-white' unstained regions, was assessed visually by recording the presence or absence of the amide I-III peaks (at 1660, 1554 and 1240 cm^{-1}, respectively) and the carbonate peak at 1400-1450 cm^{-1} (Paschalis et al., 2017).

To assess the extent of diagenetic alterations of the different regions of bone ('red/orange', 'dark' and 'unstained', as described above), two peak ratios were calculated for each spectrum. Peak height measurements were taken in Spectragryph following advanced baseline correction. The carbonate to phosphate (C/P) ratio was calculated as the ratio of absorbance of the ν_3 CO_3 peak height at *ca.* 1417 cm^{-1} to the ν_3 phosphate PO_4 peak height at *ca.* 1035 cm^{-1} (as defined by Wright and Schwartz, 1996; Kontopoulos et al., 2018). The amide to phosphate ratio (Am/P) was calculated by dividing the height of the ν_1 amide peak at *ca.* 1640 cm^{-1} by the height of the main ν_3 phosphate peak at *ca.* 1035 cm^{-1} (Kontopoulos et al., 2018). The weight % organic content of bone was calculated using the equation wt % organic = 11.06 ln (Am/P) + 32.43 (according to Trueman et al., 2004). Values for both ratios and the weight % organic content were averaged for each of the three coloured regions for each bone. The splitting factor, which is often used to measure the extent of bone diagenesis (Weiner and Bar-Yosef, 1990), could not be calculated as data was too noisy below 800 cm^{-1} having been collected in specular reflection mode using the FTIR microscope.

3. Results

3.1. XRF

The mapping XRF allowed analysis of a large area of the bone cross section, highlighting the distribution of the elements present across the coloured layers, confirming that the orange/brown staining was associated with the presence of iron and the black layers and mottling were associated with manganese (Fig. 2). In addition, it was observed that the iron distribution was greater on the endosteal layer than the periosteal in E11525 and E781, which was the opposite to E12313. Indeed, the iron in the endosteal layer of E12313 had to be confirmed by XRF as it was not clear on visual inspection. Although iron and manganese were often observed in separate, discrete layers (as evidenced for E12313; Fig. 2h and i) they were observed together in some regions (in particular the endosteal edge of E11525; Fig. 2e and f).The XRF maps also highlight some patterns of the mineral-rich layers in the thin sections, such as the iron and manganese bands repositioning in response to a crack present by migrating further into the bone in E12313 (Fig. 2h and i).

3.2. SEM-EDS

Investigation of changes to bone histology and/or bioerosion was limited as the thin sections of bone could not be polished or coated prior to subsequent synchrotron analysis. Hence, the SEM-EDS analysis focused on the structure of the mineralised layers and the elements present. The iron and manganese layers are comprised of concentrations of the materials ranging from more irregular small specks to oval/circular shapes of high density (Fig. 3). This formed the visible bands as

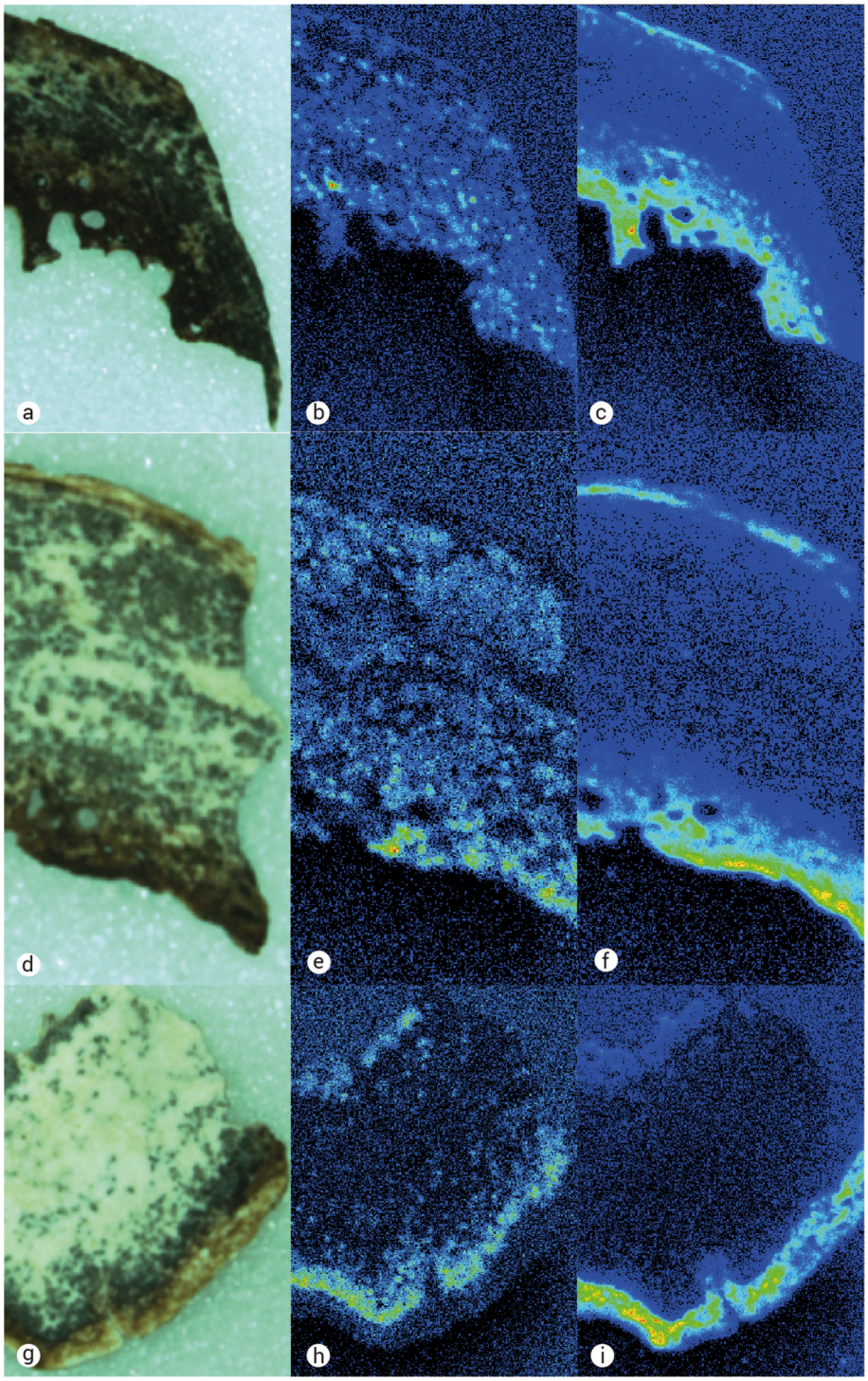

Fig. 2. XRF mapping images of thin sections of bones E781, E11525 and E12313. Images show distribution of manganese (Mn-Ka) and iron (Fe-Ka) across the bones matching the visual staining. Sample E781 is shown in Fig. 2a, with Mn and Fe elemental maps shown in Fig. 2b and c, respectively. Sample E11525 is shown in Fig. 2d, with Mn and Fe elemental maps shown in Fig. 2e and f, respectively. Sample E12313 is shown in Fig. 2g, with Mn and Fe elemental maps shown in Fig. 2h and i, respectively.

they accumulated in particular areas of the bone. The iron band was tighter in formation than the manganese band which broke up into the speckling seen across the bone. Iron and manganese were usually detected in discrete regions of the bone, and were only occasionally observed together (as also seen in the XRF maps).

Backscatter electron images (e.g. Fig. 4) illustrate the atomic contrast observed between the iron-rich layers and the surrounding bone mineral. Although the associated elemental spectra should be interpreted with caution, it would appear the levels of oxygen increased with increased iron. This was less obvious in manganese-rich areas. In some instances, damage to the bone was interpreted as being bacterially-mediated (e.g. Fig. 5) with the distribution of iron and manganese clusters matching the infilling of previous bacterial colonies (see discussion).

3.3. Micro-CT

This non-destructive technique allowed visualisation of the interior bone structure and highlighted the position of the mineralised layers. Localised regions of mineralisation could be seen within the bones for the first time, without having to section the bones. The iron-rich layers appeared at a higher greyscale density on the CT images than the

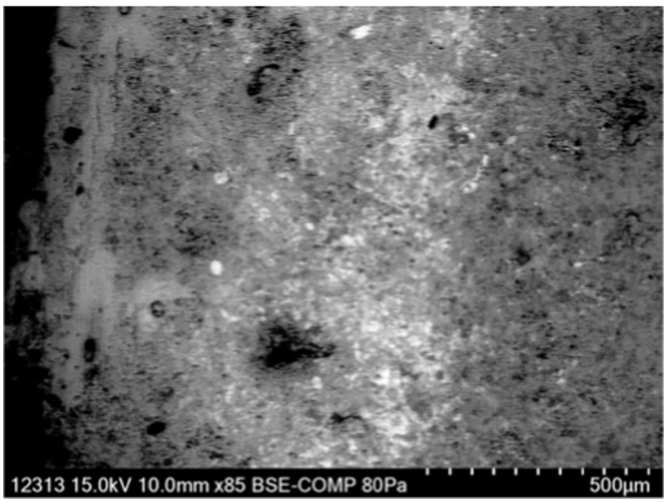

Fig. 3. Bright regions correspond with high levels of iron across the endosteal edge of bone E12313.

manganese-rich regions, but both were clearly distinguishable from the bone mineral (Fig. 6). The images clearly show the mineralisation patterns observed visually and with both XRF and SEM-EDS, namely intermittent layers of iron underneath the visibly-unaltered buff-coloured external surface, with manganese layers beneath the iron ones. When more trabecular bone was present on the endosteal surface of the bone, this also contained iron.

The CT scans of the three Etton bones showed E12313 had the most distinct mineralised layers and E781 the least, as expected from visual observation. E12313 had clear sections of manganese mineralisation around the medullary cavity (Fig. 6b). The iron and manganese in E12313 was not evenly distributed around the endosteal portion, but was concentrated to one side of the bone (Fig. 6a).

The smaller fragment of E781 (Fig. 6d) showed bands of iron that appear to have started forming in slightly different areas of the bone, as if the layer formation was repositioning within the bone over time. E781 had the clearest example of this iron band activity.

It was clear from a visual inspection of particular bone fragments (Fig. 7) that the mineralised layers continued to run parallel to, and at the same depth from, the surface edge of some large breaks as observed around the unbroken periosteal surface edge of the bone.

The intermittent distribution of iron and, to a lesser extent, manganese, underneath the surface indicates that mineral ingress did not necessarily occur from the open, broken ends of the bone. A nutrient foramen is a channel within the bone used for blood vessels in life. As a hollow soon after deposition it acts similarly to a 'crack' known to be present at time of burial and the CT showed it acted as a focus for the iron deposits in the bone (Fig. 6c). Other cracks into the bone were seen disrupting the iron layers in a similar, if not as extensive, way (e.g. Fig. 6b), while other cracks showed no effect on the layers present (Fig. 6e).

3.4. FTIR

The FTIR data was interrogated in two different ways to assess the difference in diagenetic alteration between the three differently stained regions within the bone: the red/orange, iron-rich areas, the dark-coloured manganese-rich regions, and the off-white unstained areas. Example spectra are presented in Fig. 8.

Firstly, the presence of bone organic and crystalline components in the different stained regions were investigated by visual comparison of amide and carbonate peaks with those of a thin section of well-preserved archaeological bone. No significant difference was observed in either amide or carbonate peak presence and clarity between the differently stained regions across the bones when these stained sections were compared to each other. For example, given the SEM-EDS results showing lower calcium in regions of high iron it could be hypothesised that the bone mineral and perhaps the collagen had been negatively

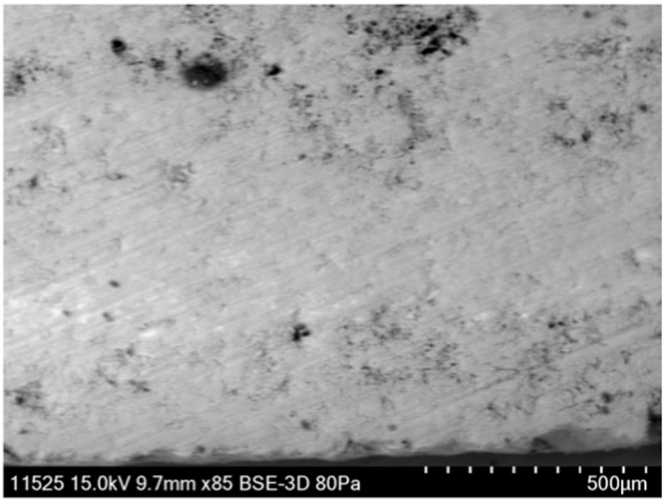

Fig. 5. Outer edge of bone 11,525, showing regions assumed to be associated with bacterial colonies.

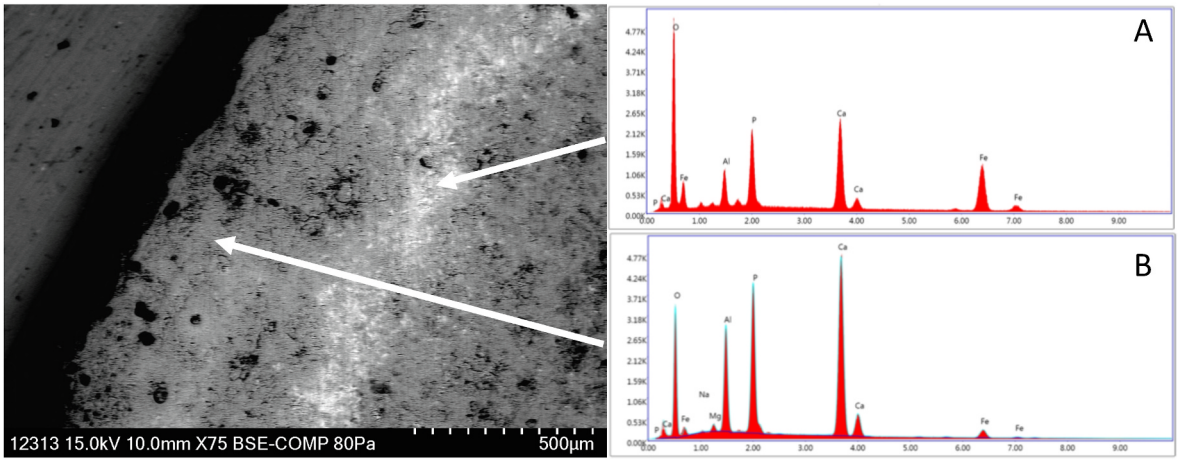

Fig. 4. Backscatter electron imaging illustrates the atomic number contrast showing the band of iron-rich material (A) relative to the bone matrix (B) in E12313.

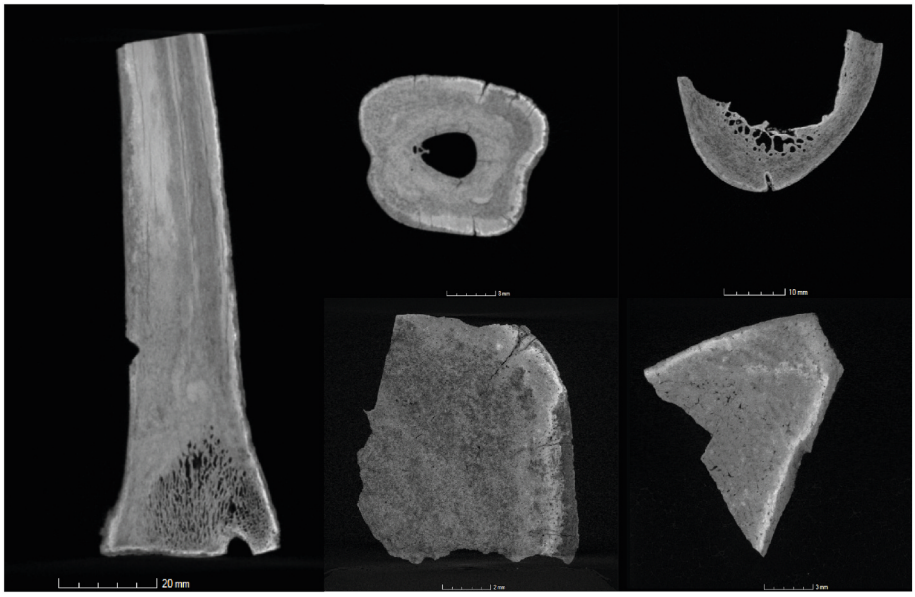

Fig. 6. Micro-CT images of bone, with high density (brightest) regions representing iron mineralisation, and medium level density correlating with manganese mineralisation, in contrast to the unmineralized bone. Clockwise from left: a: E12313 longitudinal section (indentation on left-hand bone surface can be seen on Fig. 1g); b: E12313 cross section; c: E11525, showing nutrient foramen; d: E781, showing 'repositioning' of iron layer; e: E12313, showing a crack from the external surface passing through the iron and manganese layers.

Fig. 7. Bones from Etton (not E12313, E11525, E781), showing post-mortem breakages.

affected in the red/orange, iron-rich regions but there was no significant difference seen between the iron layer and the buff-coloured exterior to support this. This may be a product of too small a sample size, or sensitivity of the scale and measurements. Between the bones themselves however, there was a noted difference in the peaks. Collagen preservation (as indicated by the amide peaks) was greatest in E12313, although peak height (and hence amount present) varied across the sample. In comparison with the other two bones, E781 had the poorest collagen preservation, but the highest carbonate peaks.

The carbonate to phosphate (C/P) and amide to phosphate (Am/P) peak ratios are given in Table 1. Natural biogenic carbonate in bone has a C/P ratio of ~0.34–0.36 (Nielsen-Marsh, 1997; Hollund et al., 2017). The loss of carbonate due to post-depositional recrystallisation and hydroxyapatite alterations results in the lowering of this value (Stiner et al., 1995), as seen for all regions except for the dark region in E12313. The red/orange regions in E11525 and E12313 had the lowest C/P ratios, indicating that the hydroxyapatite was the most altered in the iron-rich regions, but the C/P values were consistent across all three regions in E781. The average C/P ratio for the dark regions of E12313 was elevated, at 0.43, indicating that the hydroxyapatite was altered with an additional carbonate (possibly calcite) present (Nielsen-Marsh and Hedges, 2000).

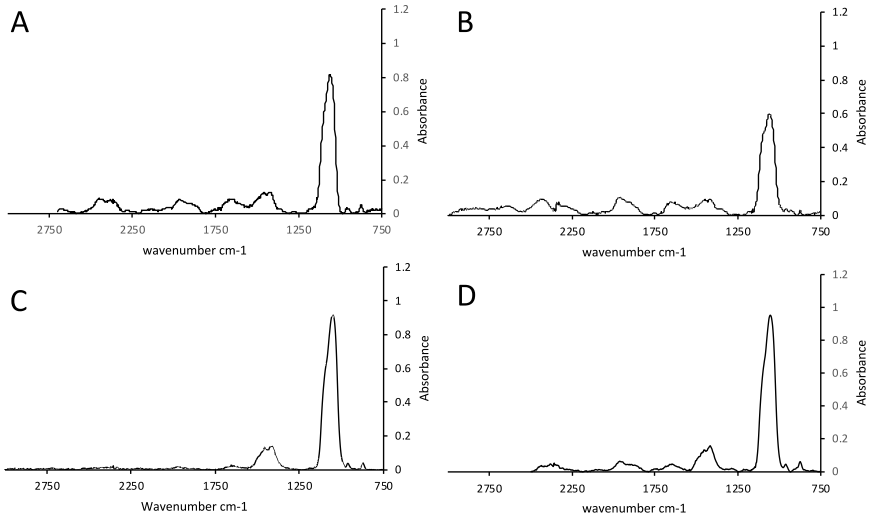

Fig. 8. Example FTIR spectra: A: white unstained region of E11525; B: dark, manganese-rich region of E12313; C: white unstained region of E781, with no amide peak; D: red/orange iron-rich region of E12515.

Table 1
Average C/P, Am/P and weight % organic content for the three different coloured stained regions in the three mineralised bones from Etton.

Bone	C/P			Am/P			Wt % organic content		
	Dark	White	Red/Orange	Dark	White	Red/Orange	Dark	White	Red/Orange
E781	0.17	0.17	0.16	0.15	0.04	0.05	11.6	0	0
E11525	0.20	0.23	0.18	0.24	0.34	0.13	16.8	20.5	9.6
E12313	0.43	0.20	0.18	0.43	0.27	0.13	23.1	17.9	9.7

The Am/P ratio of bones decreases with collagen loss (Hollund et al., 2017). The least amount of collagen was detected in the red/orange iron-rich regions for E11525 and E12313. Virtually no collagen remained in either the white, unstained or red/orange areas of E781. Fig. 8C shows a typical spectrum for a white, unstained region of E781 with the amide peak at 1640 cm^{-1} absent. The average Am/P ratio of 0.43 for the dark, manganese-rich region of E12313 was considerably higher than the other regions (as well as the average for fresh modern bone of 0.32; Hollund et al., 2017). Given that fresh modern bone contains ca. 22% collagen (van Klinken, 1999), combined with the elevated C/P ratio for this region of E12313, it is possible that some, or all, of the amide peaks at 1640 cm^{-1} were incorrectly identified. In many of these particular spectra the region from ca. 1660 to 1630 cm^{-1} was noisy (especially after baseline correction) with no clear amide peak, in contrast to spectra of a well-preserved archaeological bone collected under the same conditions where the amide peak was clearly visible at ca. 1640 cm^{-1}.

3.5. Evidence of bone degradation

E781 was different to the E12313 and E11525 bones for a number of reasons. Micro-CT analysis revealed curvilinear lines of lower density running across the fragment of bone, which was not seen in any other Etton bone, even at a greater resolution (Fig. 9). These ripples could indicate plexiform bone, which has been recorded around the periosteal edge in cattle and other animal bone (Hillier and Bell, 2007; Turner-Walker et al., 2002).

SEM images showed cracking which, while it occurred in all the Etton bones, was most prominent in E781. E781 broke in thin sectioning and required a greater number of FTIR scans to produce reliable spectra (to account for signal to noise ratio). All this, as well as the lack of amide peaks in the FTIR spectra, is suggestive of a greater extent of degradation in this bone compared to the other two.

4. Discussion

The excavation report for Etton Causewayed Enclosure states that 'Bones from the upper levels …of the enclosure ditch were a pale buff colour, mineralised, and generally poorly preserved' while 'Bones from the primary ditch deposits were stained a deep brown colour, unmineralized, and well preserved' (Pryor, 1998). Although the bone ID numbers reported here (E11525, E12313, E781) could not be matched to a specific ditch/context within the report, the pale buff description suggests the bones in this study were from the enclosure ditch. However, these bones exhibited a much more complex pattern of iron and manganese mineralisation than the excavation report suggests. The pale buff-coloured periosteal surface layer overlies an intermittent red/-brown coloured iron-rich layer above a black manganese-rich layer, with black manganese-rich 'speckling' throughout the cortical bone. On the endosteal surface is an iron layer, overlying a manganese layer further within the bone; these two layers 'overlap' more than at the periosteal surfaces of E781 and E11525. The iron and manganese compounds are mostly likely oxides or oxyhydroxides.

The ditch from which the bones were likely excavated was affected by fluctuations in groundwater, as well as seasonal flooding caused by subsequent alluviation. The water levels at the site would also have lowered following the formation of the 'Maxey Cut', a drainage feature introduced at some point in the Medieval period (Pryor, 1998). The mineralisation observed within the bones appears likely to have occurred through a complex cycle of processes likely driven by changes in redox conditions caused by the fluctuating groundwater levels over several millennia during burial, as well as environmental changes during excavation and over three decades of post-excavation storage.

The processes involved at Etton Causewayed Enclosure are assumed to be similar to those proposed by Reiche et al. (2003) for bones buried in sands above the water table but exposed to fluctuating redox conditions due to precipitation and occasional flooding at the Neolithic site of

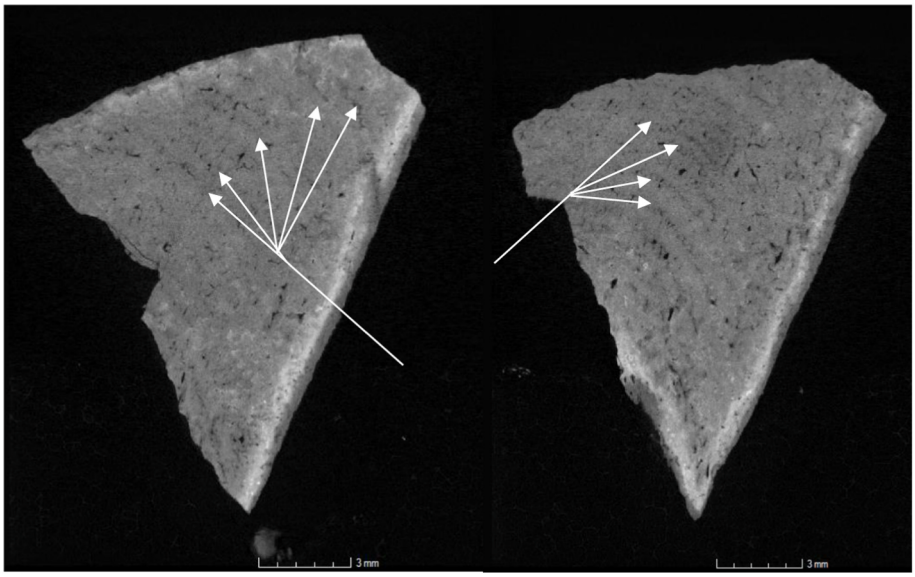

Fig. 9. Micro-CT scan images showing variations in bone density across a small fragment of E781.

Bercy, France. The bones from Bercy have elevated iron concentrations at the interior and exterior edges of the bone (detected by PIXE analysis), with irregular manganese flecking within the bone section, but the mineralisation does not appear to be as extreme as in the bones at Etton, and nor do the Bercy bones have the additional manganese layers beneath the iron layers at the bones' surface (Reiche et al., 2003, Fig. 2).

During periods when the water table had dropped at Etton, the aerobic conditions would have supported rapid microbial degradation of the bones' organic matter. Although detailed histological analysis was not undertaken as part of this study, SEM-EDS analysis did indicate bioerosion had occurred (e.g. Fig. 5). As the water table fluctuated and the bones were once again submerged, short-chain, degraded collagen would have leached out of the bone due to its increased solubility (Collins et al., 1995), resulting in a further increase in porosity within the bone, allowing iron- and manganese-rich porewaters (Pryor, 1998) to penetrate deeper into the bones' structure. The influx of porewater into regions which had already undergone collagen degradation and associated increases in porosity is known to promote the dissolution and recrystallisation of the bone hydroxyapatite mineral phase, resulting in increased crystal size and the potential incorporation of exogeneous ions into the hydroxyapatite lattice (Nielsen-Marsh and Hedges, 2000). Once the groundwaters subsided and the environment became oxidising again, manganese and iron oxides and oxyhydroxides formed within the voids created by the bacterial activity.

Given the unusual multiple coloured layers and speckled patterns observed within these bones today, it is perhaps surprising that the bones were described simply as 'mineralised' in the excavation report (Pryor, 1998), with no further detail or photographs. This omission suggests that while mineralisation likely started during burial, it probably continued during the washing/drying stages post-excavation, and possibly also during over three decades of storage. It is possible that some (or even all) of the iron and/or manganese bands may have been formed during the drying of the bones, where the inner parts were still wet and anoxic, but the outer regions of bone were dry and oxic.

The location of the mineralised layers immediately beneath the endosteal and periosteal surfaces of the Etton bones correlates with bands of bacterial bioerosion observed in archaeological bone (Booth et al., 2016; Fernández-Jalvo et al., 2010). The mineralisation often resembles the rounded shapes of bacterial colonies spreading out across the bone (Fig. 5), matching the description of microscopical focal destruction (Hackett, 1981; White and Booth, 2014). The 'speckled' distribution of manganese within the cortical bone is similar to the pattern of bioerosion in mineralised collaged described by Turner-Walker (2019, and references therein) whereby bacterial activity expands and enlarges the canalicular system, and the manganese oxide infill of canaliculi and other voids, as well as non-Wedl foci produced by bacterial activity, described by Elliot and Grime (1993) and Dal Sasso et al. (2014).

While the position of the mineral formation within the bones can therefore be seen to correlate with bacterial bioerosion, the formation of the manganese layers further into the bone than the iron layers on both the periosteal and endosteal surfaces remains unclear. Stratification of minerals based on redox potential of the environment has been noted for sediments, where manganese and iron will separate and form distinct layers, but the manganese oxide layer normally occurs above the iron oxide layer (e.g. Ingri and Pontér, 1986). The mineralisation appears to have occurred through one or more cycles of bacterial degradation under aerobic conditions, followed by the influx of iron (Fe^{2+}) and manganese (Mn^{2+}) under reducing conditions as groundwaters rose, and subsequent precipitation of iron and manganese oxides when the water table fell and conditions were once again oxidising. However, the potential role of manganese oxidising bacteria in promoting mineralisation associated with bacterial decay cannot be completely discounted (and may even be responsible for the unexpected positioning of the manganese layer beneath the iron layer). Although still poorly understood, manganese oxidising bacteria are known to play an integral role in the biogeochemical cycling of several elements, including manganese, iron and carbon, and are ubiquitous in nature, including at oxic-anoxic interfaces and within ferromanganese nodules (Tebo et al., 2005; Carmichael et al., 2013).

The extent of mineralisation varied between the three bones. More iron and manganese was observed on the XRF maps of the endosteal layer than the periosteal layer of E11525 and E781, in contrast to E12313. Both E11525 and E781 had more visible manganese content distributed throughout the bone cross section than E12313. The greatest differences in mineralisation were observed between bones E12313 and E781. E11525 was the intermediate bone in terms of both mineral distribution and concentration. E781 had a very diffuse manganese layer compared to the other two bones, with an evenly distributed iron-rich layer around the bone. In contrast, the iron-rich layer in E12313 was much more prominent on one side (Fig. 6a and b), although the cause of this is unclear. It is possible that the bone was buried at the wet-dry boundary, with only the lower part of the bone submerged, but ground water tables are seldom that stable. Alternatively, this could have been caused by a gravity effect, whereby water had drained from the uppermost part of the bone and accumulated within the lower part, either during burial or post-excavation drying.

The XRF maps and micro-CT images revealed differences in mineral layer formation relative to cracks and fractures in the bone. The nutrient foramen is the only large channel travelling along/through the bone that was definitely known to be present at the time of burial. When observed on the micro-CT scans for bones E11525 and E781, the nutrient foramen has a very high concentration of iron around its edge or just below the surface and clearly acted as conduit for the iron into the bone, corresponding to Elliot and Grime's (1993) observation that iron more typically fills the larger pores in the bone matrix such as Haversian canals, and lines its cortical surfaces.

In some instances, the mineral layer was observed to have formed parallel to the edge of the crack, travelling into the bone away from the surface, indicating that mineralisation occurred around a pre-existing crack (Fig. 6c). Fig. 2g–i and 6b (E12313), clearly show the iron layer penetrating into the bone along the edge of a crack, but the crack continues beyond the layer, suggesting the crack was widened after the mineral layer formed. The manganese layer also follows the same crack but is seen on the XRF maps to be more scattered and weaker around the crack than around the main edge of the bone. It is possible that the formation of the crack allowed oxygen and/or porewaters further into the bone, allowing for dissolution and reprecipitation of the mineral layers as the redox conditions changed. In other instances, the cracks break through the layers without affecting the path of the mineralised band, indicating that they formed after the mineralisation had occurred. These cracks are likely taphonomic damage associated with prolonged burial and/or subsequent excavation and analysis, or possibly formed after drying out of the bone after the excavation and later storage.

Variations in the extent of degradation in the bones may indicate that the Etton bones were deposited at different times, or may represent different micro-environments with different redox conditions depending on their position within the ditch. E781 appears most diagenetically altered, E12313 the least. E781 had the most surface cracks visible by SEM-EDS, and was the hardest bone to section as it kept breaking and had the lowest C/P ratio and Am/P ratios in all three differently stained regions (red/orange, dark, unstained). It was the only bone to show 'ripples' across the surface of the bone in the micro-CT images (Fig. 9). If this is the plexiform bone separating as we believe, then this happening only in E781 suggests a weakening of the bone structure as it draws apart from its concentric layers (Hillier and Bell, 2007). This plexiform bone is normally associated with specific animal species; given E781 was not identified to species from visual examination of the bone fragment this information highlights another benefit of non-destructive micro-CT imaging. Overall, E12313 had the most amount of collagen surviving (based on the amide peaks), but collagen preservation was variable across the bone.

For all three bones, the C/P and Am/P ratios indicated that the regions of iron mineralisation (i.e. the red/orange areas) were the most diagenetically altered and contained the least collagen. However, the manganese-rich regions (i.e. dark/black stained areas) still contained some collagen, and the C/P ratio was similar to the white regions of the bone, which also contained some collagen in some bones. This may support Elliot and Grime's (1993) observation that manganese mineralisation occurs in smaller voids than iron mineralisation does, and hence more original bone material is present in the dark-stained regions than the red/orange ones. Although the FTIR focused on a 50 × 50 μm area, the section was 300 μm thick, so the differences in ratios may simply reflect mineral variations at depth within the thin sections.

5. Conclusion

The three bones from Etton Causewayed Enclosure studied here demonstrate a complex pattern of diagenetic alteration and mineralisation. The shaping of the iron-rich (red/orange) and manganese-rich (dark) layers follow the typical form of archaeological bacterial degradation of periosteal and endosteal surface bioerosion but the extent of the iron and manganese oxide and oxyhydroxide formation, and in particular the positioning of the manganese layer below the iron layer, is different to that described in bones from any other site, to the authors' knowledge. This mineralisation is likely to have started during burial, due to groundwater fluctuations causing repeated cycling between reducing and oxidising conditions. Bacterial activity during aerobic periods left voids within the bone, in particular under the bone surface and expanding the canaliculi network within the cortical bone, into which iron and manganese-rich groundwater penetrated. These then precipitated as oxides and oxyhydroxides once the groundwater levels dropped and oxygen became available. The mineralisation process likely continued post-excavation, especially during the washing and drying and possibly also during long-term storage.

Although histological details were not studied here, this study highlighted the use of micro-CT for the visualisation of mineralisation (especially iron) within intact bone, as well as plexiform bone separation.

This study was undertaken as a precursor to synchrotron analysis to investigate the relationship between collagen preservation/degradation and mineralisation on the micro- and nano-scale, and whether mineralisation occurs solely by replacement within voids or also through substitution within the hydroxyapatite bone mineral.

Author contributions

Charlotte Loy: Validation, Formal Analysis, Data curation, Writing – Original draft preparation. **Fiona Brock:** Conceptualization, Methodology, Writing – review & editing, Supervision. **Chris Dyer:** Methodology, Writing – review & editing, Supervision.

Data availability

The underlying data related to this article can be accessed at https://doi.org/10.17862/cranfield.rd.21753605.

Declaration of competing interest

The authors declare that they have no known competing financial interests or personal relationships that could have appeared to influence the work reported in this paper.

Acknowledgements

The Natural History Museum, London, and Roberto Portela Miguez (senior curator in charge of mammals), are thanked for providing the samples from Etton Causewayed Enclosure, and allowing destructive analysis. Charles French provided invaluable insights into Etton Causewayed Enclosure and post-excavation processing of the bones. Bronwen Evans and Carole Elford are thanked for use of the microtome in their research lab in the School of Medicine, University of Cardiff. David Lane and Jon Painter are also thanked for their support with the XRF and SEM-EDS analysis, respectively, which was undertaken during the lead author's MSc research project at Cranfield Forensic Institute. Clare Pratchett (Cranfield University) is thanked for help producing the figures for this manuscript. Bradley Tebo (University of California – San Diego) is thanked for his guidance on redox stratification. The anonymous reviewers of the initial draft of this paper are gratefully thanked for their feedback, which significantly improved this article.

References

Badone, E., Farquhar, R.M., 1982. Application of neutron activation analysis to the study of element concentration and exchange in fossil bones. J. Radioanal. Chem. 69, 291–311.

Booth, T.J., Redfern, R.C., Gowland, R.L., 2016. Immaculate conceptions: micro-CT analysis of diagenesis in Romano- British infant skeletons. J. Archaeol. Sci. 74, 124–134. https://doi.org/10.1016/j.jas.2016.08.007.

Breuning-Madsen, H., Holst, M.K., Rasmussen, M., 2001. The chemical environment in a burial mound shortly after construction—an archaeological–pedological experiment. J. Archaeol. Sci. 28, 691–697.

Carmichael, M.J., Carmichael, S.K., Santelli, C.M., Strom, A., Bräuer, S.L., 2013. Mn(II)-oxidizing bacteria are abundant and environmentally relevant members of ferromanganese deposits in caves of the Upper Tennessee River Basin. Geomicrobiol. J. 30, 779–800. https://doi.org/10.1080/01490451.2013.769651.

Child, A.M., 1995. Towards an understanding of the microbial decomposition of archaeological bone in the burial environment. J. Archaeol. Sci. 22, 165–174.

Collins, M.J., Riley, M.S., Child, A.M., Turner-Walker, G., 1995. A basic mathematical simulation of the chemical degradation of ancient collagen. J. Archaeol. Sci. 22, 175–183.

Dal Sasso, G., Maritan, L., Usai, D., Angelini, I., Artioli, G., 2014. Bone diagenesis at the micro-scale: bone alteration patterns during multiple burial phases at Al Khiday (Khartoum, Sudan) between the Early Holocene and the II century AD. Palaeogeogr. Palaeoclimatol. Palaeoecol. 416, 30–42. https://doi.org/10.1016/j.palaeo.2014.06.034.

Elliot, T.A., Grime, G.W., 1993. Examining the diagenetic alteration of human bone material from a range of archaeological burial sites using nuclear microscopy. *Nucl. Instrum. Methods Phys. Res.* B 77, 537–547.

Fernández-Jalvo, Y., Andrews, P., Pesquero, D., Smith, C., Marín-Monfort, D., Sanchez, B., Geigl, E., Alonso, A., 2010. Early bone diagenesis in temperate environments Part I: surface features and histology. Palaeogeogr. Palaeoclimatol. Palaeoecol. 288, 62–81. https://doi.org/10.1016/j.palaeo.2009.12.016.

Hackett, C.J., 1981. Microscopical focal destruction (tunnels) in excavated human bones. Med. Sci. Law 21, 243–265.

Hedges, R.E.M., 2002. Bone diagenesis: an overview of processes. Archaeometry 44, 319–328. https://doi.org/10.1111/1475-4754.00064.

Henne, A., Craw, D., Gagen, E., Southam, G., 2021. Biologically facilitated precipitation of metals in low-Fe waters at the sulphidic Mount Chalmers mine, Queensland, Australia. Ore Geol. Rev. 136, 104238 https://doi.org/10.1016/j.oregeorev.2021.104238.

Herwartz, D., Tütken, T., Jochum, K.P., Sander, P.M., 2013. Rare earth element systematics of fossil bone revealed by LA-ICPMS analysis. Geochem. Cosmochim. Acta 103, 161–183. https://doi.org/10.1016/j.gca.2012.10.038.

Hillier, M.L., Bell, L.S., 2007. Differentiating human bone from animal bone: a review of histological methods. J. Forensic Sci. 52 (2), 249–263. https://doi.org/10.1111/j.1556-4029.2006.00368.x.

Hollund, H.I., Teasdale, M.D., Mattiangeli, V., Sverrisdóttir, O.Ó., Bradley, D.G., O'Connor, T., 2017. Pick the right pocket. Sub-Sampling of bone sections to investigate diagenesis and DNA preservation. Int. J. Osteoarchaeol. 27, 365–374. https://doi.org/10.1002/oa.2544.

Ingri, J., Pontér, C., 1986. Iron and manganese layering in recent sediments in the Gulf of Bothnia. Chem. Geol. 56, 105–116.

Jans, M.M.E., 2010. Microbial bioerosion of bone – a review. In: Wisshak, M., Tapanila, L. (Eds.), Current Developments in Bioerosion. Springer, Berlin, pp. 397–413.

Kendall, C., Eriksen, A.M.H., Kontopoulos, I., Collins, M.J., Turner-Walker, G., 2018. Diagenesis of archaeological bone and tooth. Palaeogeogr. Palaeoclimatol. Palaeoecol. 491, 21–37.

Kiseleva, D., Shilovsky, O., Shagalova, E., Ryanskayaa, A., Chervyakovskayaa, M., Pankrushinaa, E., Cherednichenkoa, N., 2019. Composition and structural features of two Permian parareptile (*Deltavjatia vjatkensis*, Kotelnich Site, Russia) bone fragments and their alteration during fossilisation. Palaeogeogr. Palaeoclimatol. Palaeoecol. 526, 28–42. https://doi.org/10.1016/j.palaeo.2019.04.015.

Kontopoulos, I., Presslee, S., Penkman, K., Collins, M.J., 2018. Preparation of bone powder for FTIR-ATR analysis: the particle size effect. Vib. Spectrosc. 99, 167–177. https://doi.org/10.1016/j.vibspec.2018.09.004.

Marín-Arroyo, A.B., Landete-Ruiz, M.D., Vidal-Bernabeu, G., Seva Román, R., González Morales, M.R., Straus, L.G., 2008. Archaeological implications of human-derived

manganese coatings: a study of blackened bones in El Mirón Cave, Cantabrian Spain. J. Archaeol. Sci. 35 (3), 801–813. https://doi.org/10.1016/j.jas.2007.06.007.
Nielsen-Marsh, C.M., 1997. Studies in Archaeological Bone Diagenesis. Unpublished PhD dissertation, University of Oxford.
Nielsen-Marsh, C.M., Hedges, R.E.M., 2000. Patterns of diagenesis in bone I: the effects of site environments. J. Archaeol. Sci. 27, 1139–1151. https://doi.org/10.1006/jasc.1999.0537.
Nielsen-Marsh, C.M., Smith, C.I., Jans, M.M.E., Nord, A., Kars, H., Collins, M.J., 2007. Bone diagenesis in the European Holocene II: taphonomic and environmental considerations. J. Archaeol. Sci. 34 (9), 1523–1531. https://doi.org/10.1016/j.jas.2006.11.012.
Paschalis, E.P., Gamsjaeger, S., Klaushofer, K., 2017. Vibrational spectroscopic techniques to assess bone quality. Osteporos. Int. 28, 2275–2291. https://doi.org/10.1007/s00198-017-4019-y.
Pryor, F., 1998. Etton: Excavations at a Neolithic Causewayed Enclosure Near Maxey, Cambridgeshire, 1982-7. English Heritage Archaeological Report 18.
Reiche, I., Favre-Quattropani, L., Vignaud, C., Bocherens, H., Charlet, L., Menu, M., 2003. A multi-analytical study of bone diagenesis: the Neolithic site of Bercy (Paris, France). Meas. Sci. Technol. 14, 1608–1619.
Stiner, M.C., Kuhn, S.I., Weiner, S., Bar-Yosef, O., 1995. Differential burning, recrystallization, and fragmentation of archaeological bone. J. Archaeol. Sci. 22, 223–237.
Tebo, B.M., Johnson, H.A., McCarthy, J.K., Templeton, A.S., 2005. Geomicrobiology of manganese (II) oxidation. Trends Microbiol. 13 (9), 421–428. https://doi.org/10.1016/j.tim.2005.07.009.
Turner-Walker, G., Nielsen-Marsh, C.M., Syversen, U., Kars, H., Collins, M.J., 2002. Sub-micron spongiform porosity is the major ultra-structural alteration occurring in archaeological bone. Int. J. Osteoarchaeol. 12, 407–414. https://doi.org/10.1002/oa.642.
Turner-Walker, G., 2019. Light at the end of the tunnels? The origins of microbial bioerosion in mineralised collagen. Palaeogeogr. Palaeoclimatol. Palaeoecol. 529, 24–38.
Trueman, C.N., Behrensmeyer, A.K., Tuross, N., Weiner, S., 2004. Mineralogical and compositional changes in bones exposed on soil surfaces in Amboseli National Park, Kenya: diagenetic mechanisms and the role of sediment pore fluids. J. Archaeol. Sci. 31, 721–729. https://doi.org/10.1016/j.jas.2003.11.003.
Trueman, C.N., Privat, K., Field, J., 2008. Why do crystallinity values fail to predict the extent of diagenetic alteration of bone mineral? Palaeogeogr. Palaeoclimatol. Palaeoecol. 266, 160–167. https://doi.org/10.1016/j.palaeo.2008.03.038.
Van Klinken, G.J., 1999. Bone collagen quality indicators for paleodietary and radiocarbon measurements. J. Archaeol. Sci. 26, 687–695.
Weiner, S., Bar-Yosef, O., 1990. States of preservation of bones from prehistoric sites in the near East: a survey. J. Archaeol. Sci. 17, 187–196. https://doi.org/10.1016/0305-4403(90)90058-D.
White, L., Booth, T.J., 2014. The origin of bacteria responsible for bioerosion to the internal bone microstructure: results from experimentally-deposited pig carcasses. Forensic Sci. Int. 239, 92–102. https://doi.org/10.1016/j.forsciint.2014.03.024.
Wright, L.E., Schwarz, H.P., 1996. Infrared and isotopic evidence for diagenesis of bone apatite at Dos Pila, Guatemala: palaeodietary implications. J. Archaeol. Sci. 23, 933–944.